Supporting information

Single-Component Rare-Earth-free White-Light-Emitting Metal-Organic Framework Towards Nitroaromatic Explosive Sensing and Dye Absorption

Yan-Wu Zhao, Bin-Xue, Nan Zhang, Li-E Guo, Sheng-Yan Zhu, Xian-Ming Zhang*

Key Laboratory of Magnetic Molecules & Magnetic Information Materials Ministry of Education, School of Chemistry & Material Science, Shanxi Normal University, Taiyuan, 030031, Shanxi, P. R. China.

Correspondence to: zhangxm@dns.sxnu.edu.cn.

Table of Contents

Experiment Section

1. Materials and chemicals

Cadmium nitrate hexahydrate ($Cd(NO_3)_2 \cdot 4H_2O$) were purchased from National drug group chemical reagents Co. Ltd.. 4,4′-Pyridine and 1,4,5,8-naphthalenetetra-carboxylic dianhydride were purchased from Aladdin reagents Co. Ltd.. CH_3CN, DMF, DMA, MeOH, EtOH, THF, aceton and CH_2Cl_2 were purchased from Sailboat Chemical Reagent Technology Co. Ltd., respectively. All of the other chemicals used were analytical reagent grade and used without further purification.

2. Measurements

All chemicals for the syntheses were commercially available reagents of analytical grade and were used without further purification. The FT-IR spectra were recorded from KBr pellets in range 400-4000 cm^{-1} on a Perkin-Elmer Spectrum BX FT-IR spectrometer. UV absorption spectra were recorded with a U-3310 spectrophotometer. Elemental analysis was performed on a Vario EL-II elemental analyzer. Powder X-ray diffraction (PXRD) data were recorded in a Bruker D8 ADVANCE powder X-ray diffractometer. The thermogravimetric analyses (TGA) were carried out in an air atmosphere using SETARAMLABSYS equipment at a heat in grate of 10°C/min. Luminescence spectra for liquid samples were recorded, and lifetime measurements were measured by a single-photon counting spectrometer using an Edinburgh FLS920 spectrometer equipped with a continuous Xe900 xenon lamp, a mF900 μs flash lamp, a red-sensitive Peltier-cooled Hamamatsu R928P photomultiplier tube (PMT), and a

closed Janis CCS-350 optical refrigerator system. The corrections of excitation and emission for the detector response were performed from 200 to 900 nm. Lifetime data were fitted with two-exponential-decay functions. The quantum yield measurements were performed using the absolute method on an Edinburgh Instrument FLS920 spectrometer equipped with a $BaSO_4$-coated integrating sphere. Scanning electron microscopic (SEM) images were obtained with a JSM-7500F operated at beam energy of 25.0 kV. The X-ray photoelectron spectroscopy (XPS) were obtained by the Thermo scientific K-Alpha$^+$ XPS with a monochromatic Al Ka X-ray source (1486.6 eV) operating at 72 W (12 kV, 6 mA). The XPS profiles were collected for the C 1s, N 1s, O 1s and Zn 2p binding energy regions. All XPS spectra underwent background subtraction and had been fitted using mixed Gaussian-Lorentzian peak shapes.

3. **Synthesis of organic compound**

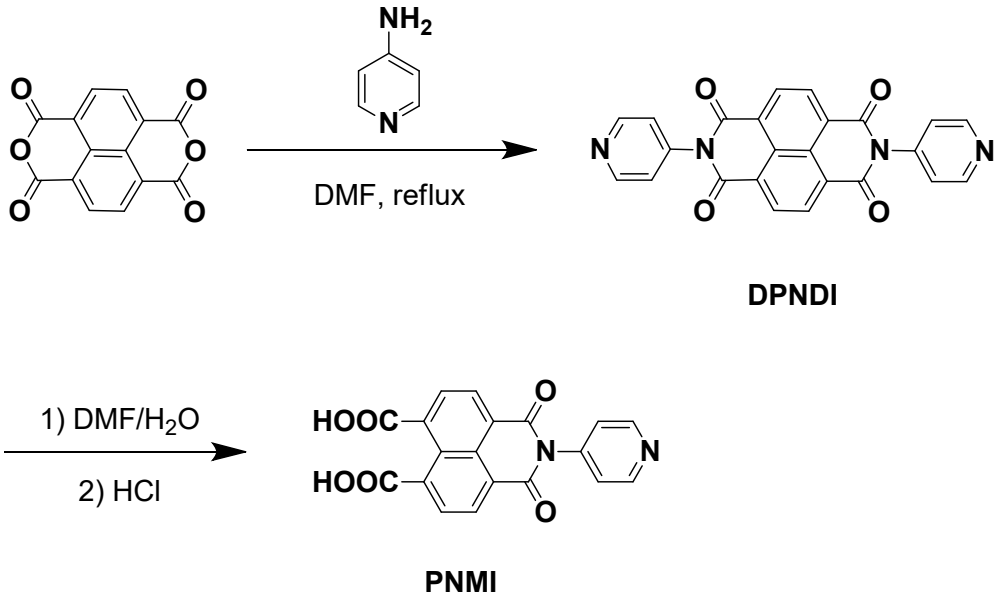

Scheme S1. the synthetic routes of **DPNDI** and **PNMI**.

3.1 Synthesis of *N,N'*-di-(4-pyridyl)-1,4,5,8-naphthalenetetracarboxydiimide (**DPNDI**)

4-aminopyridine (7.46 mmol, 710 mg) and 1,4,5,8-naphthalenetetracarboxylic dianhydride (3.73 mmol, 1 g) were added into 30 mL DMF, which was refluxed overnight under stirring. The reaction mixture was cooled to room temperature, and the precipitate was filtered, then washed with deionized water for several times, dried in a 60 ºC oven to obtain tan powder (1.06 g, yield, 67.7%). ^{1}HNMR (600 MHz, d^{6}-DMSO): δ 8.82 (d, 4H), 8.75 (s, 4H), 7.58 (d, 4H) ppm. MS (m/z) (ESI+) for $C_{24}H_{12}N_4O_4$, 421 $[M+H]^+$. FT-IR (KBr, cm^{-1}): 3420(s), 1710(s), 1672(s), 1613(w), 1571(w), 1513(w), 1448(w), 1411(w), 1337(m), 1241(m), 1193(w), 1139(w), 1108(w), 985(w), 852(w), 820(w), 772(m), 724(w), 623(m), 521(w).

3.2 Synthesis of *N*-(4-pyridyl)-1,4,5,8-naphathalenetetracarboxymonoimide (**PNMI**)

DPNDI (0.5 mmol, 21 mg) in 3 mL DMF and 1 mL H_2O was added into a 15 mL of Teflon-line stainless container. The reaction mixture was stirred at room temperature for 30 min, and then placed in an oven at 60 ºC for 1 days. The resulting brown-yellow liquid was cooled to room temperature, and then acidified to pH of 1 with 1 M HCl. The required mixture with solid precipitation was put in the refrigerator to cool, filter, wash with deionized water for several times and get the product (112.6 mg, yield, 62.2%). ^{1}HNMR (600 MHz, d^{6}-DMSO): δ 13.64 (s, 2H), 8.80 (d×d, 2H), 8.58 (d, 2H), 8.24 (d, 2H), 7.56 (d×d, 2H) ppm. MS (m/z) (ESI+) for $C_{19}H_{10}N_2O_6$, 363 $[M+H]^+$. FT-IR (KBr, cm^{-1}): 3430(s), 2923 (w), 2842 (w), 1781 (m), 1711 (s), 1657 (s), 1587 (m), 1500 (w), 1430 (w), 1380 (m), 1332 (w), 1252 (m), 1192 (w), 1159 (w), 1041 (w), 953 (w), 813 (w), 770 (m), 656 (w), 596 (w).

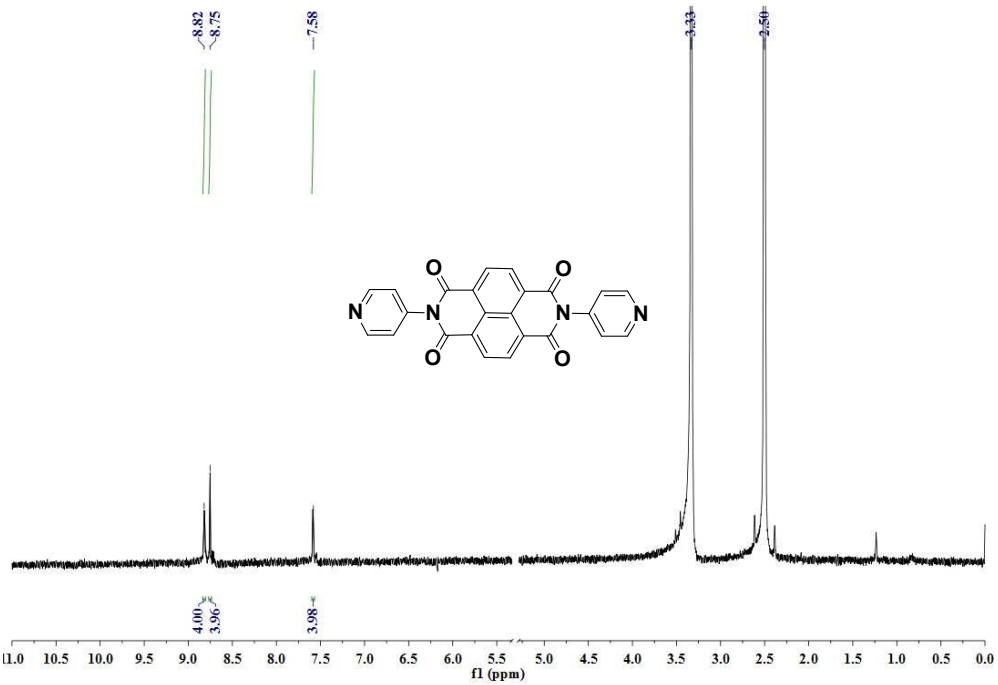

Fig. S1. [1]HNMR of *N,N′*-di-(4-pyridyl)-1,4,5,8-naphthalenetetracarboxydiimide

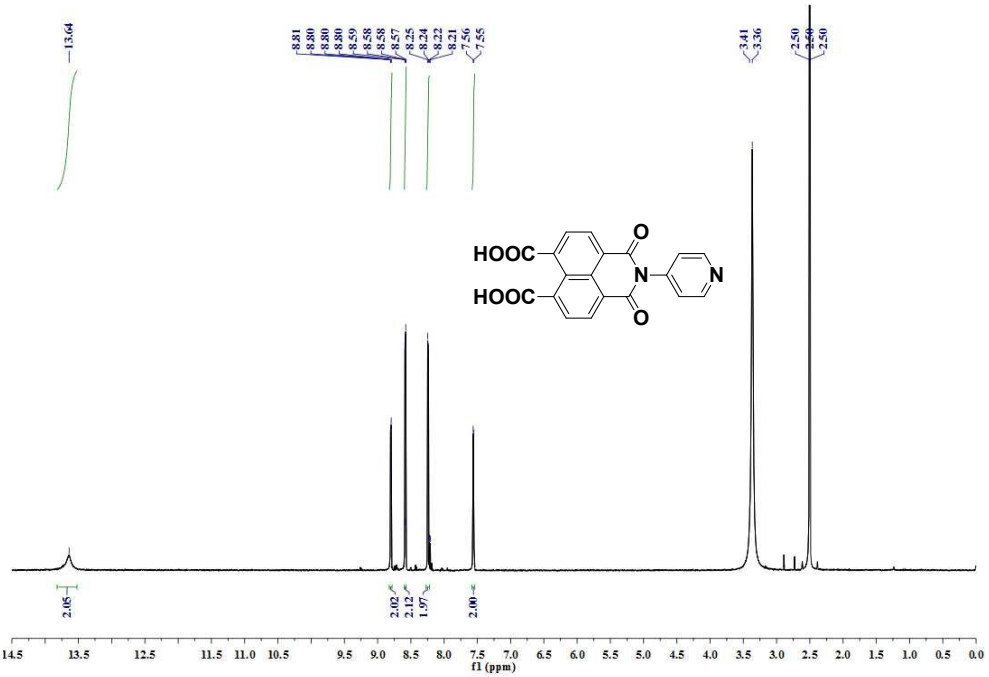

Fig. S2. [1]HNMR of *N*-(4-pyridyl)-1,4,5,8-naphathalenetetracarboxymonoimide

4. Synthesis of CdPNMI

Method 1: PNMI (0.5 mmol, 21 mg) and $Cd(NO_3)_2$•$4H_2O$ (1 mmol, 30.8 mg) were added into 3 mL DMF and 1 mL H_2O in a 15 mL Teflon-line stainless

container, respectively. The reaction mixture was stirred at room temperature for 30 min, then placed in an oven at 90℃ for 3 days, which was cooled to room temperature, filtered and washed with acetone to obtain yellow crystals with 90% yield (based on PNMI).

Method 2: DPNDI (0.5 mmol, 21 mg) and $Cd(NO_3)_2$•$4H_2O$ (1 mmol, 30.8 mg) were added into 3 mL DMF and 1 mL H_2O in a 15 mL Teflon-line stainless container, respectively. Then, 2mmol benzoic acid (24 mg) was added to the solution in batches. The reaction mixture was stirred at room temperature for 30 min, then placed in an oven at 90℃ for 3 days. The resulting mixture was cooled to room temperature, filtered and washed with acetone to obtain yellow crystals with 95% yield (based on DPNDI). Anal. Calcd for $C_{19}H_8N_2O_6Cd$ (%): C, 48.28%; H, 1.71 %; N, 5.93%. Found: C, 48.36%; H, 1.69%; N, 5.98%. FT-IR (KBr pellet, cm^{-1}): 3468(s), 2919(w), 2858(w), 1715(m), 1667(s), 1608(s), 1592(s), 1507(w), 1443(m), 1385(s), 1241(m), 1183(w), 1092(w), 969(w), 868(w), 820(w), 778(m), 628(w), 506(w).

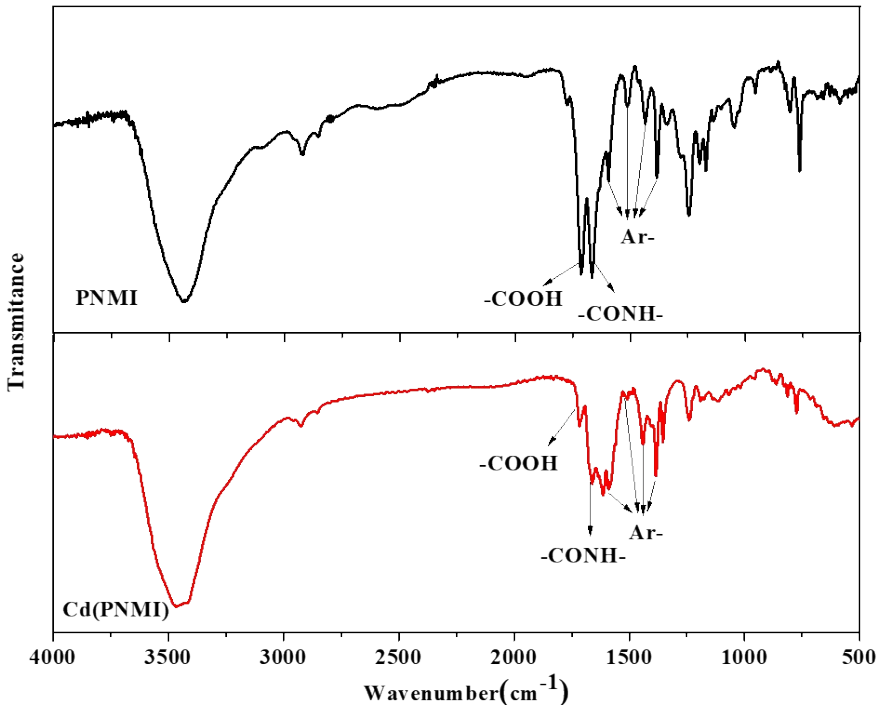

Fig. S3 IR spectra of the organic ligand PNMI and MOFs Cd(PNMI)

Structure Description and Crystal data

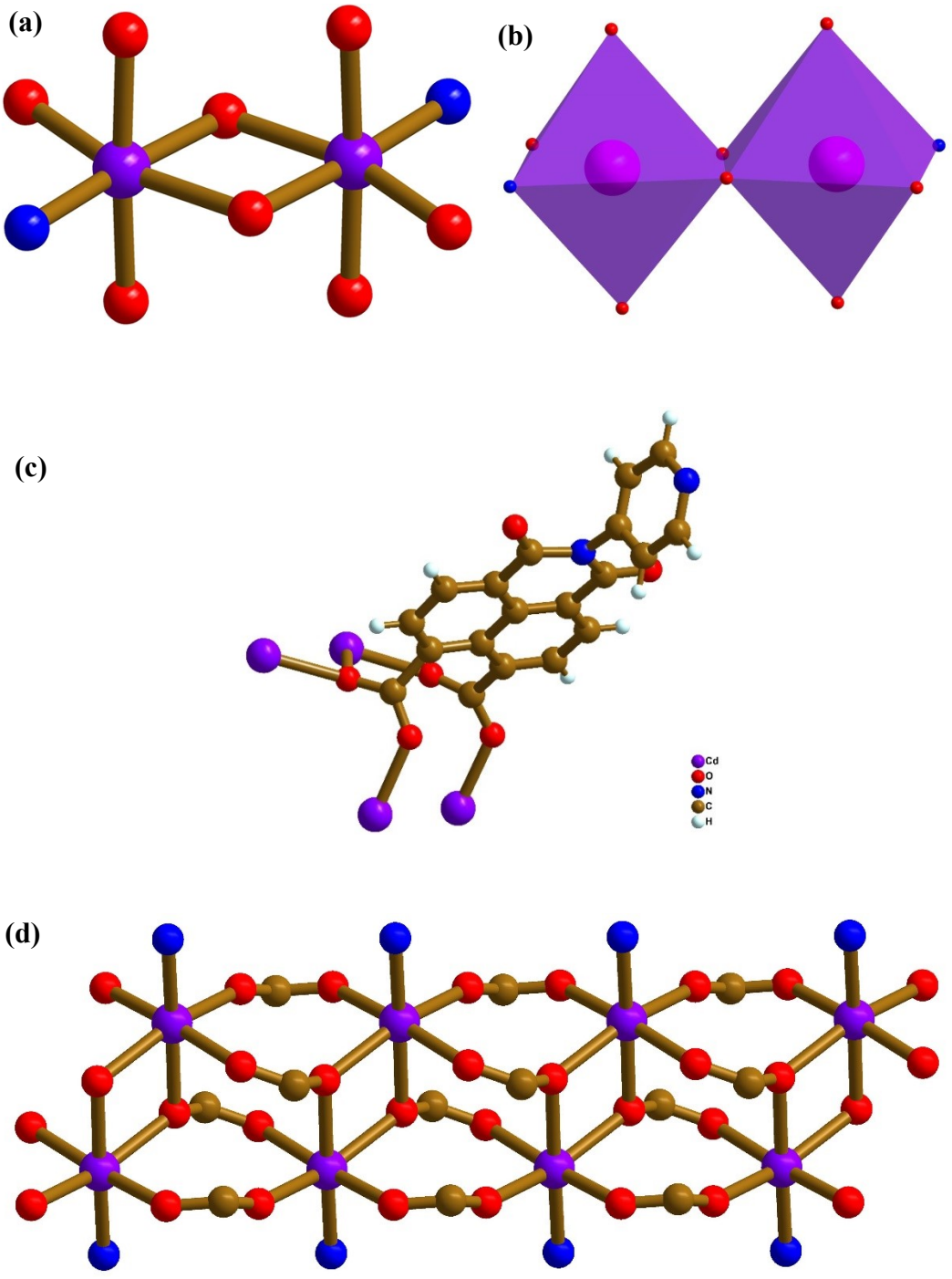

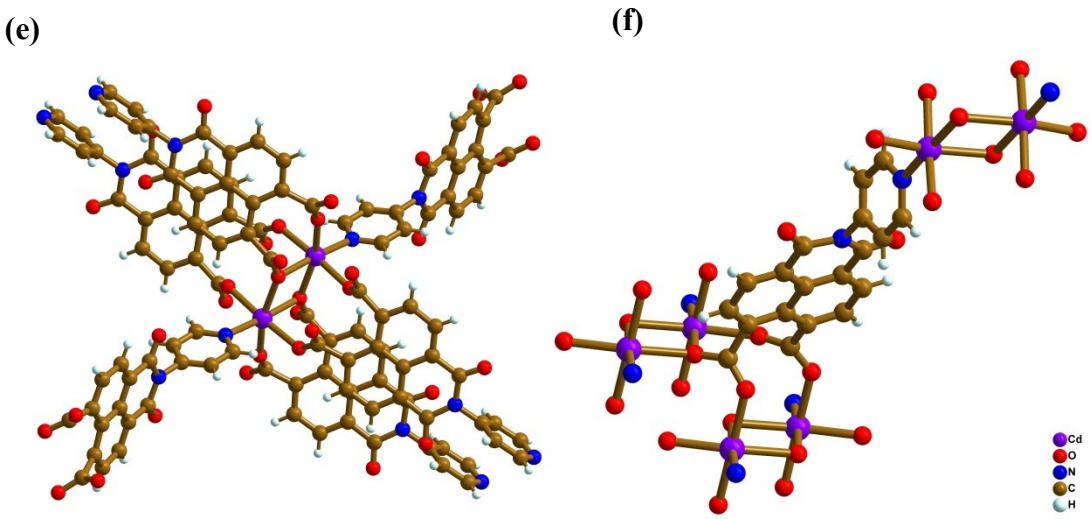

Fig. S4. (a) a $Cd_2O_8N_2$ cluster formed by two CdO_5N octahedrons; (b) the octahedron of $Cd_2O_8N_2$ cluster with a share side; (c) the coordination mode of the carboxylic group in a PNMI ligand; (d) 1D chain structure generated by $Cd_2O_8N_2$ clusters; (e) the $Cd_2O_8N_2$ cluster coordinated to six ligands; (f) the ligand coordinated to three cluster.

Table S1 Crystal data and refinement parameters for CdPNMI.

Parameters	CdPNMI
Empirical formula	$C_{19}H_8N_2O_6Cd$
Formula weight	472.67
Temperature/K	293(2)
Crystal system	monoclinic
Space group	$P2_1/n$
a/Å	5.0417(2)
b/Å	25.2931(9)
c/Å	20.3733(10)
α (°)	90
β (°)	96.179(4)
γ (°)	90
Volume (Å^3)	2582.91(19)
Z	4
Calculated density (g/cm^3)	1.216
Absorption coefficient (mm^{-1})	0.873
F(000)	928.0
Crystal size/mm^3	0.11 × 0.1 × 0.09
Radiation	MoKα (λ = 0.71073)
2Θ range for data collection/°	6.75 to 50.02
Index ranges	$-5 \le h \le 5$, $-16 \le k \le 30$, $-19 \le l \le 24$
Reflections collected	10284
Independent reflections	4519 [R_{int} = 0.0573, R_{sigma} = 0.0954]
Data/restraints/parameters	4519/0/253
Goodness-of-fit on F^2	0.912
Final R indexes [I>=2σ (I)]	R_1= 0.0428, wR_2 = 0.0619
Final R indexes [all data]	R_1= 0.0652, wR_2 = 0.0669
Largest diff. peak/hole / e Å^{-3}	0.65/-0.52

Table S2 Bond lengths [Å] and angles [º] for CdPNMI.

Cd(1)-O(1)	2.213(3)
Cd(1)-O(2b)	2.260(3)
Cd(1)-O(3a)	2.260(2)
Cd(1)-O(4c)	2.347(3)
Cd(1)-O(4b)	2.329(3)
Cd(1)-N(2e)	2.278(3)
Cd(1d)-O(2)	2.260(3)
Cd(1a)-O(3)	2.260(2)
Cd(1c)-O(4)	2.347(3)
Cd(1d)-O(4)	2.329(3)
Cd(1a)-N(2)	2.277(3)
O(1)-Cd(1)-O(2b)	82.14(9)
O(1)-Cd(1)-O(3a)	174.97(9)
O(1)-Cd(1)-O(4b)	86.32(9)
O(1)-Cd(1)-O(4c)	92.89(9)
O(1)-Cd(1)-N(2e)	95.64(11)
O(2b)-Cd(1)-O(3a)	96.98(9)
O(2b)-Cd(1)-O(4b)	83.62(10)
O(2b)-Cd(1)-O(4c)	163.11(10)
O(2b)-Cd(1)-N(2e)	99.64(12)
O(3a)-Cd(1)-O(4b)	88.66(9)
O(3a)-Cd(1)-O(4c)	86.56(9)
O(3a)-Cd(1)-N(2e)	95.64(11)

O(4b)-Cd(1)-O(4c)	79.95(10)
N(2e)-Cd(1)-O(4c)	96.90(12)
N(2e)-Cd(1)-O(4b)	176.39(12)
Cd(1d)-O(4)-Cd(1c)	100.06(10)

Symmetry transformations used to generate equivalent atoms:

a) -X, 1-Y, 1-Z; b) -1+X, +Y, +Z; c) 1-X, 1-Y, 1-Z; d) 1+X, +Y, +Z; e) 1/2-X, 1/2+Y, 1/2-Z;

Morphology of CdPNMI crystal

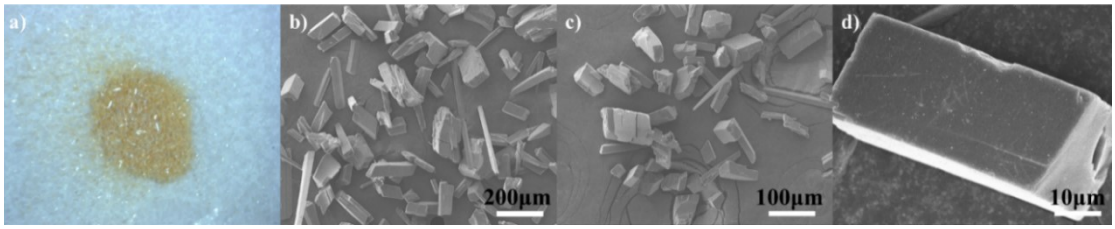

Fig. S5 optical photographs of CdPNMI crystal, a); SEM image of as-synthesized CdPNMI crystal, b-d)

XPS spectra

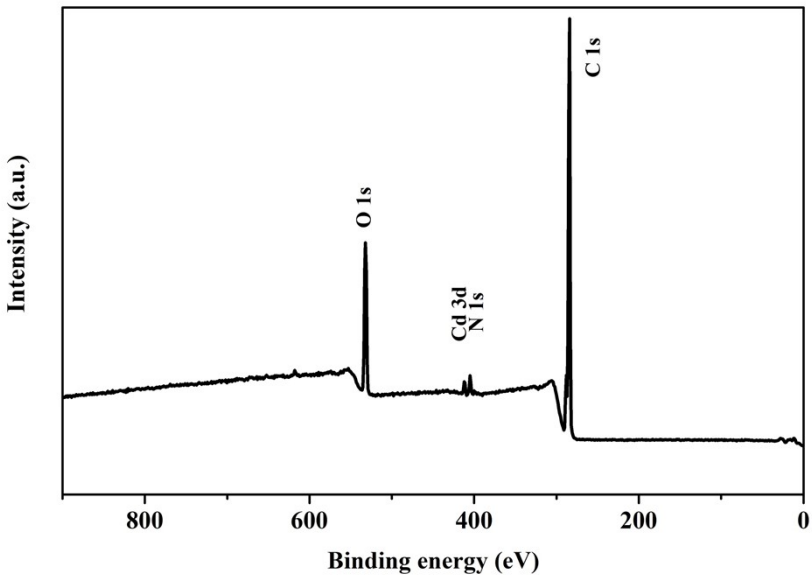

Fig. S6 XPS survey spectra of CdPNMI crystal:

PXRD of CdPNMI crystal

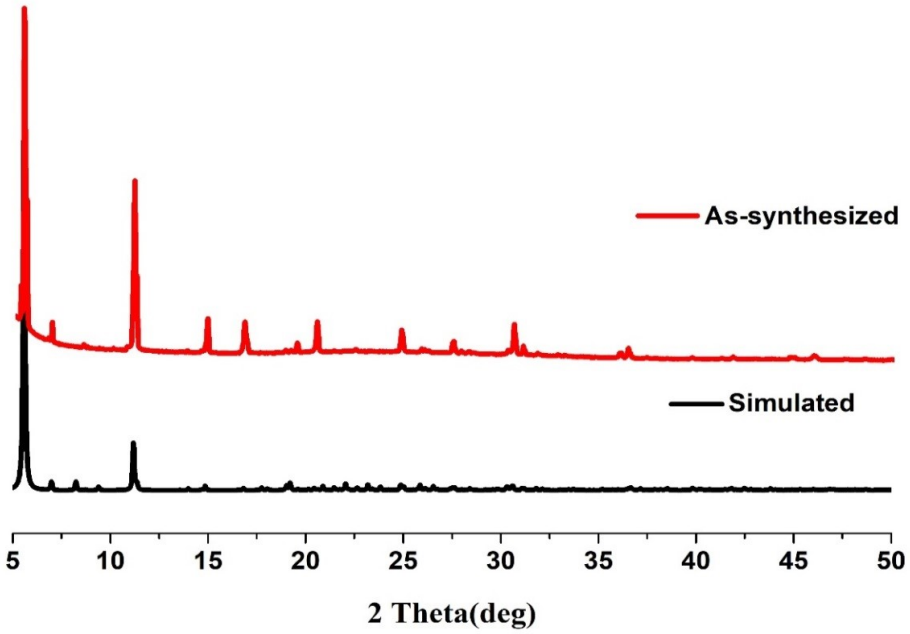

Fig. S7 Simulated PXRD and PXRD patterns of CdPNMI

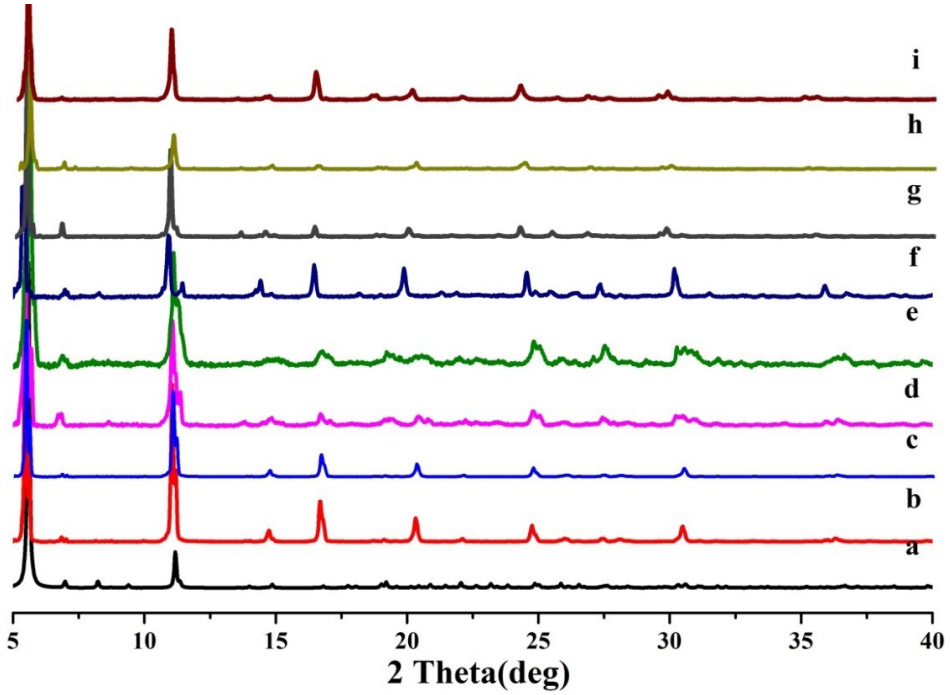

Fig. S8 Powder X-ray diffraction patterns of (a) simulated CdPNMI, (b) as-synthesized CdPNMI, and (c–i) CdPNMI after immersion in (c) CH_2Cl_2, (d) CH_3CN, (e) acetone, (f) DMA, (g) EtOH, (h) MeOH, and (i) THF

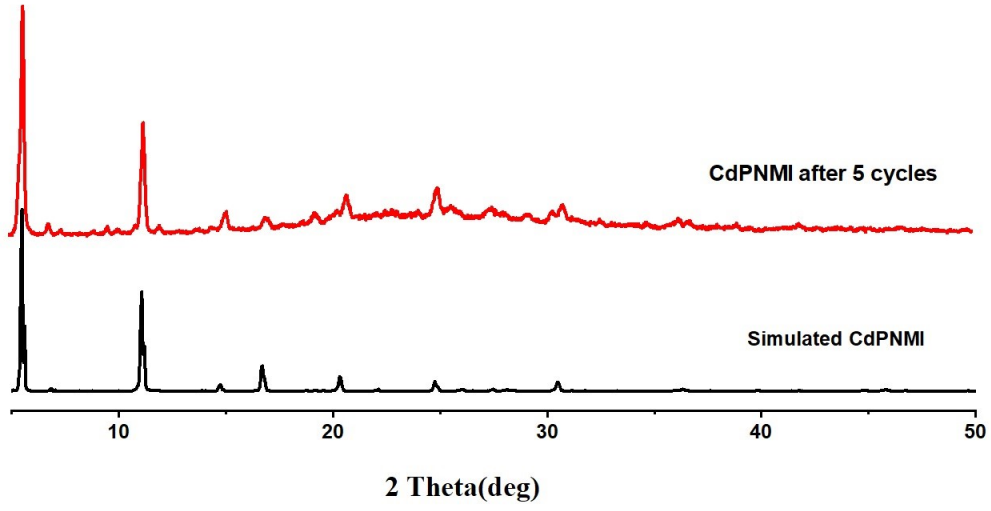

Fig. S9 Powder X-ray diffraction patterns of CdPNMI, including simulated CdPNMI (black) and CdPNMI after 5 cycles (red).

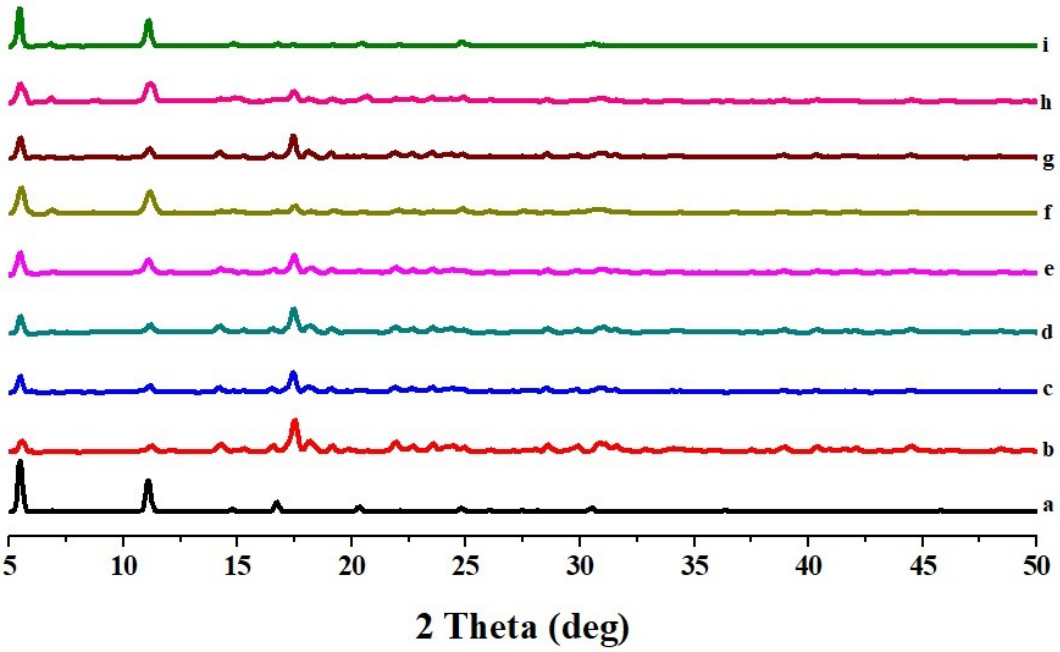

Fig. S10 PXRD of CdPNMI crystal after absorbing different concentration of RhB in acetone. (a) simulated CdPNMI (black), (b) RhB (red), (c) 5 mg L^{-1} (blue), (d) 10 mg L^{-1} (atrovirens), (e) 15 mg L^{-1} (pink), (f) 20 mg L^{-1} (brownish green), (g) 25 mg L^{-1}(brown), (h) 50 mg L^{-1} (red) and (i) 100 mg L^{-1} (green).

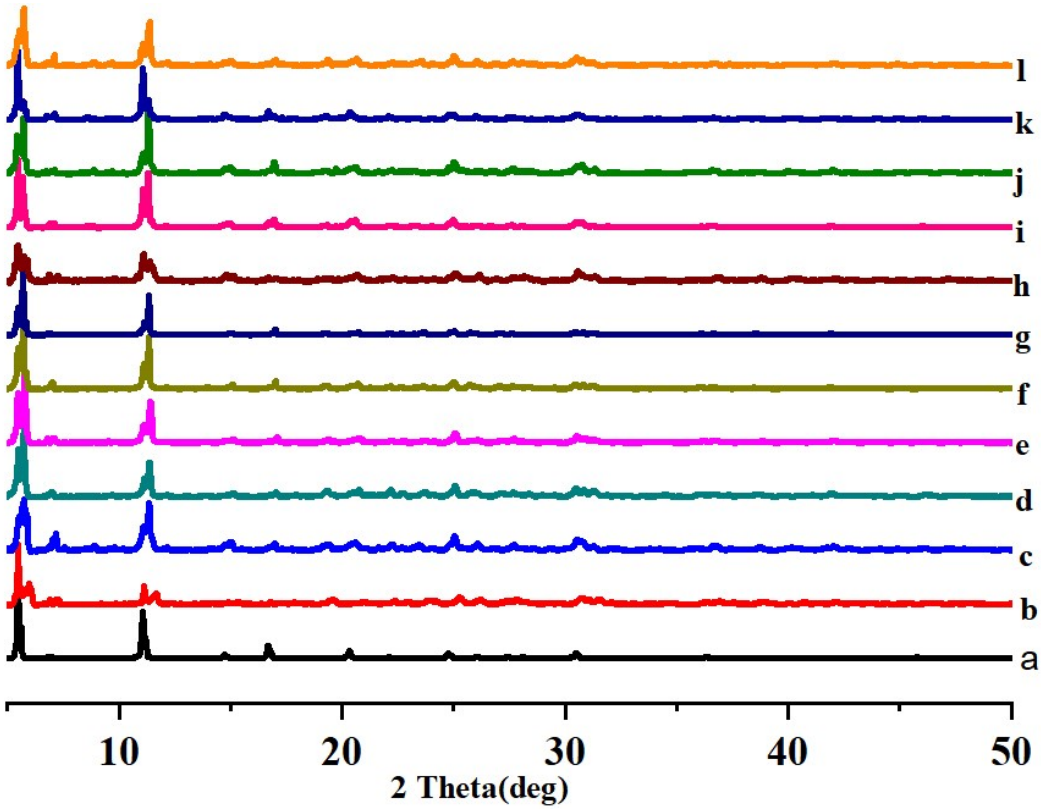

Fig. S11 PXRD of CdPNMI crystal after absorbing different concentration of FITC in

acetone. (a) simulated CdPNMI (black), (b) 50 mg L^{-1} (red), (c) 100 mg L^{-1} (blue), (d) 150 mg L^{-1} (atrovirens), (e) 200 mg L^{-1} (pink), (f) 250 mg L^{-1} (brownish green), (g) 300 mg L^{-1} (navy blue), (h) 350 mg L^{-1} (brown), (i) 400 mg L^{-1} (pinkish red), (j) 450 mg L^{-1} (green), (k) 500 mg L^{-1} (dark blue), (l) 550 mg L^{-1} (orange).

TGA curves of CdPNMI crystal

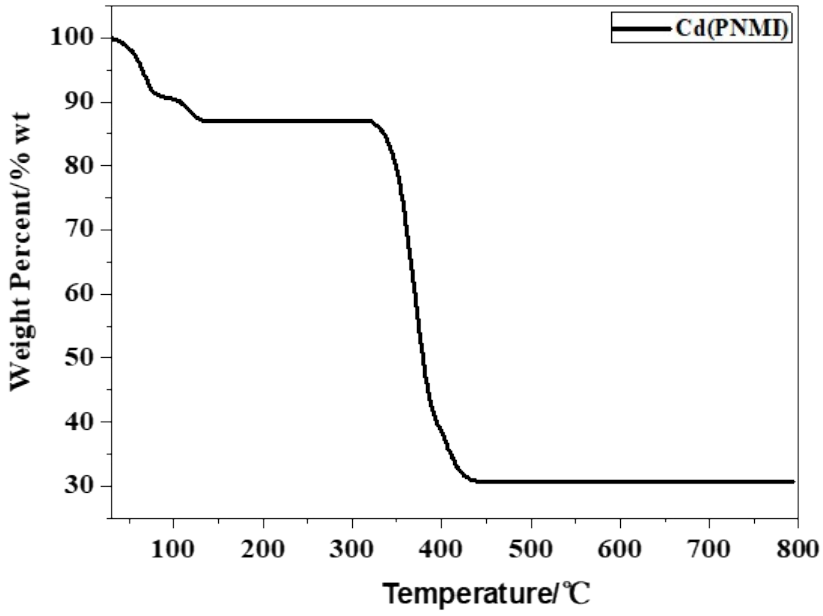

Fig. S12 TGA curves of CdPNMI

UV absorption spectra

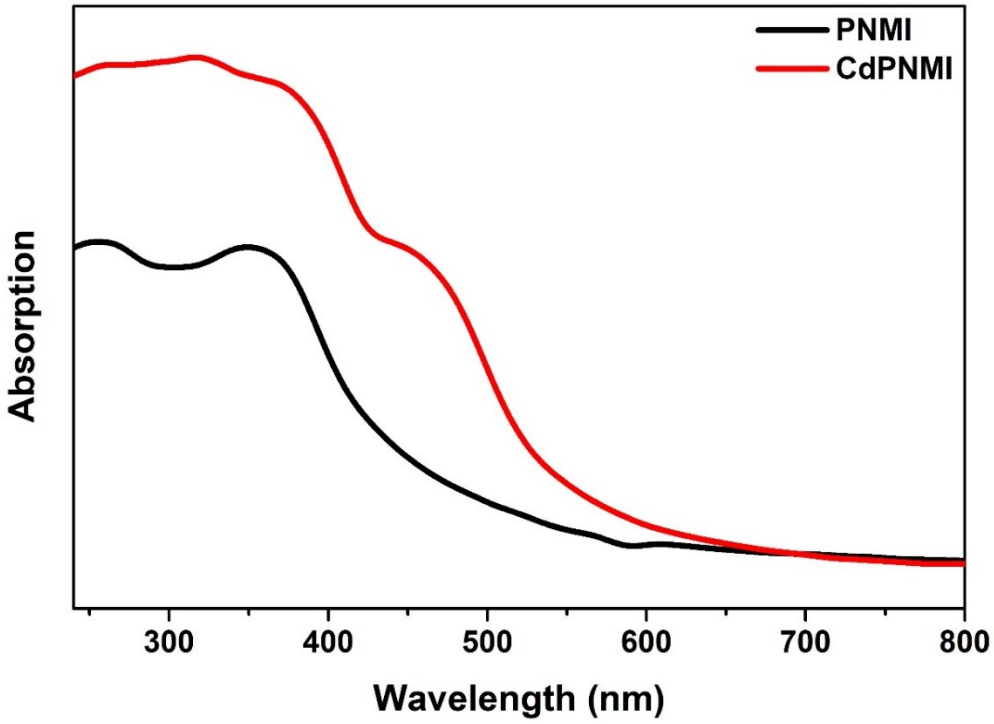

Fig. S13 UV absorption of the solid CdPNMI and ligand PNMI.

Description of fluorescence properties and Preparation of CdPNMI stock solutions

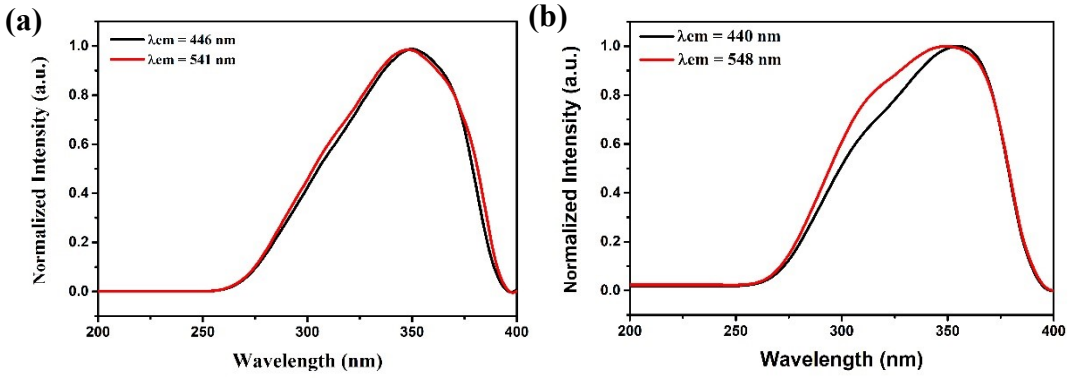

Fig. S14 The excitation spectra of PNMI ligand (a) and CdPNMI (b)

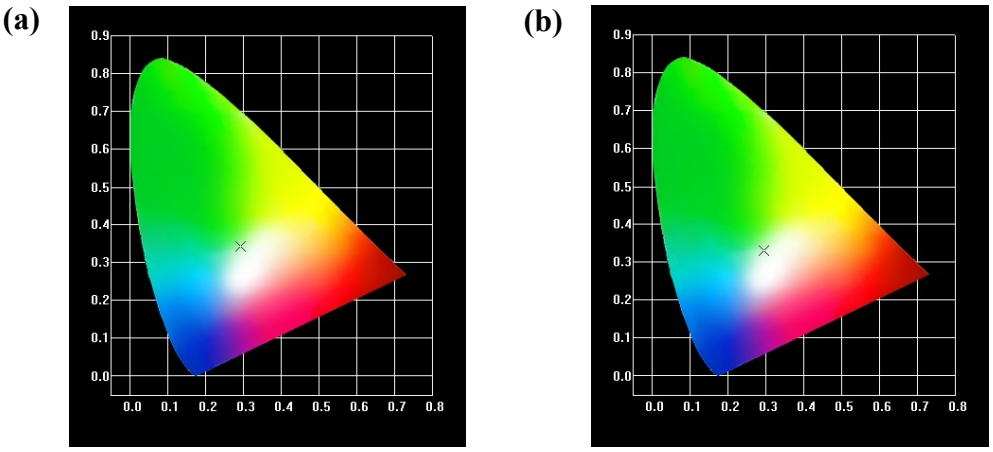

Fig. S15 The CIE (Commission Internationale de l'Eclairage) coordinates of PNMI ligand (a) and CdPNMI (b)

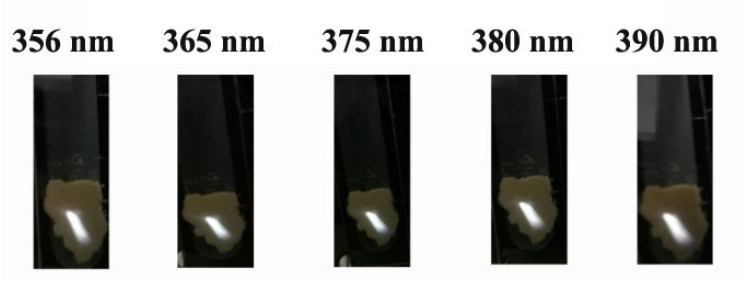

Fig. S16 CdPNMI crystal emit bright white light under different exciting light of 356, 365, 375, 380 and 390 nm.

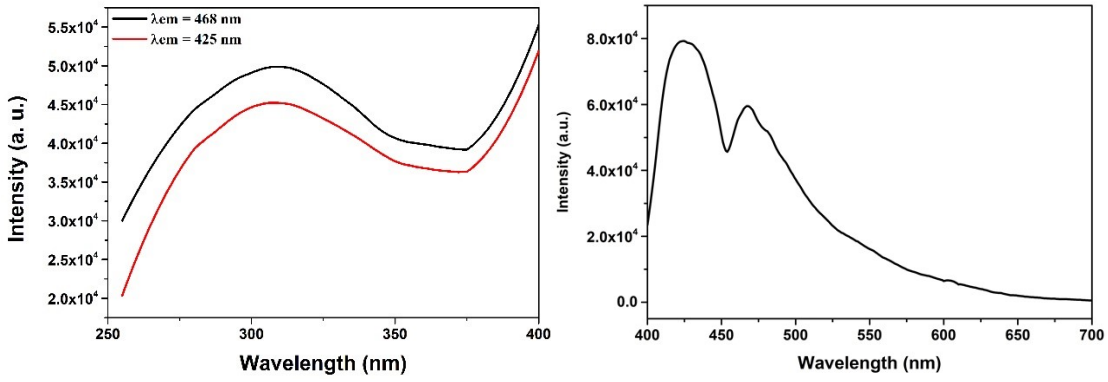

Fig. S17 Fluorescence excitation (left) and emission spectra (right) of CdPNMI emulsion in DMA.

Preparation of CdPNMI stock solutions: 5 mg of CdPNMI crystals were placed in a vial with 3 mL DMA, which was mechanically crushed by vigorous stirring overnight. The resulting white emulsion was then diluted with DMA to 50 mL for fluorescence measurements of nitroaromatic compounds. Exactly 3 mL of newly prepared CdPNMI stock solution was added to a quartz cuvette for each fluorescence experiment.

Measurement of fluorescence spectroscopy: Before measurements on fluorescence spectra of CdPNMI and probed nitroaromatic compounds, stock solution of CdPNMI and quencher nitroaromatic compound in DMA was prepared. The mixed CdPNMI and nitroaromatic compound stock solution was ultrasounded for 10 min before fluorescence measurements to give sufficient time for the diffusion of quencher through the 3D MOFs pores. An intensity reading was performed before the addition of nitroaromatic compound solutions and again after each addition of the quencher, and the slit widths of both source and detector for the excitation and the emission were kept at 2.0 nm to maintain consistency. It is noted that every measuring experiment was repeated for three times.

The quenching efficiency was defined by $(I_0-I)/I_0 \times 100\%$, where I_0 and I are the fluorescence intensity of CdPNMI emulsion before and after the addition of analytes, respectively.

The quenching constant was obtained by the Stern–Volmer (SV) equation: $I_0/I = 1+K_{SV}[Q]$, where I_0 and I are the fluorescence intensity of CdPNMI emulsion before and after the addition of quenchers, respectively, K_{SV} and [Q] represent the quenching constant (M^{-1}) and the concentration of quenchers (μM), respectively.

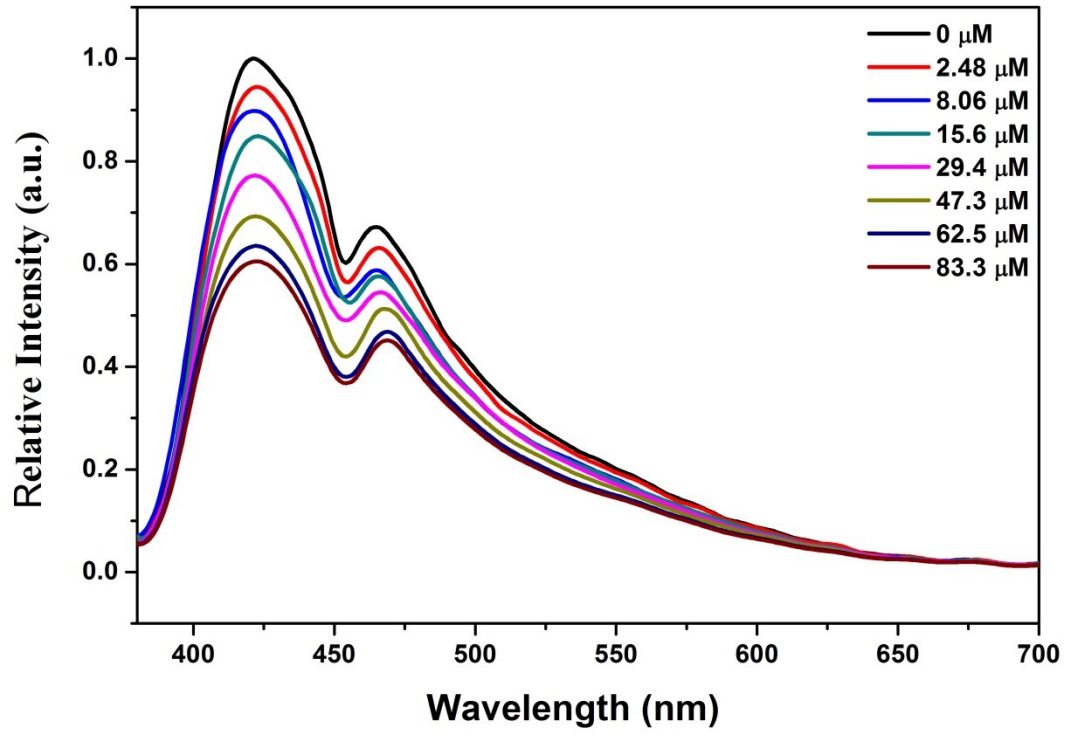

Fig. S18 Fluorescence emission profile of CdPNMI emulsion to NB with gradual concentration increasement of NB.

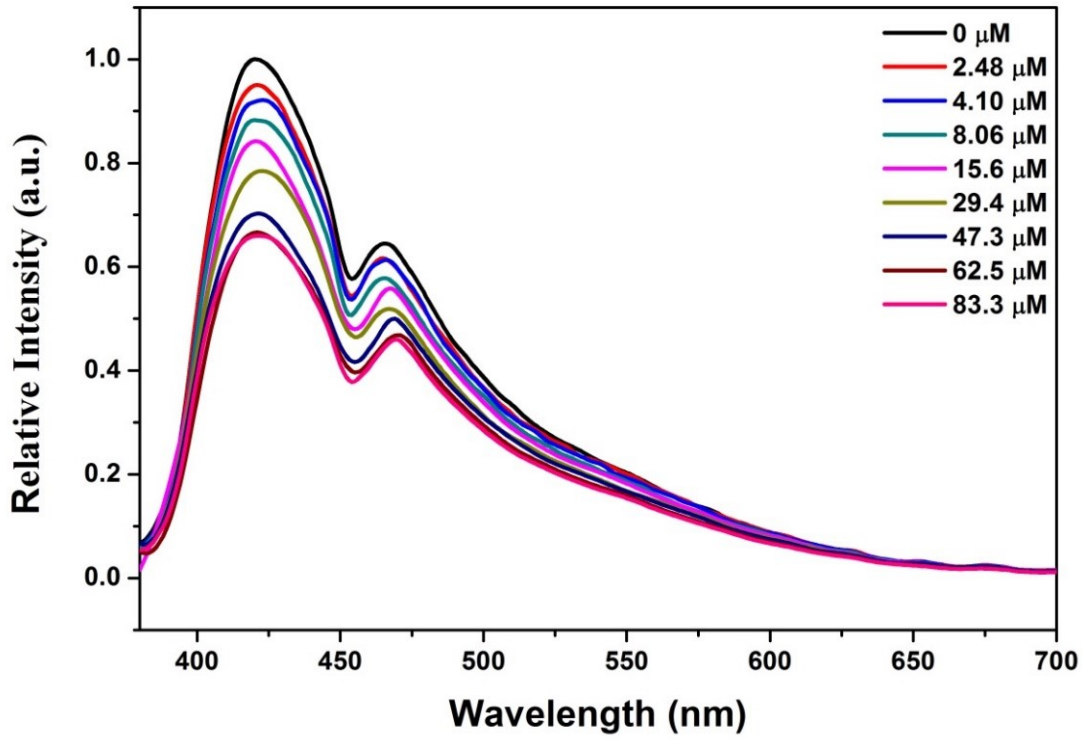

Fig. S19 Fluorescence emission profile of CdPNMI emulsion to NT with gradual concentration increasement of NT.

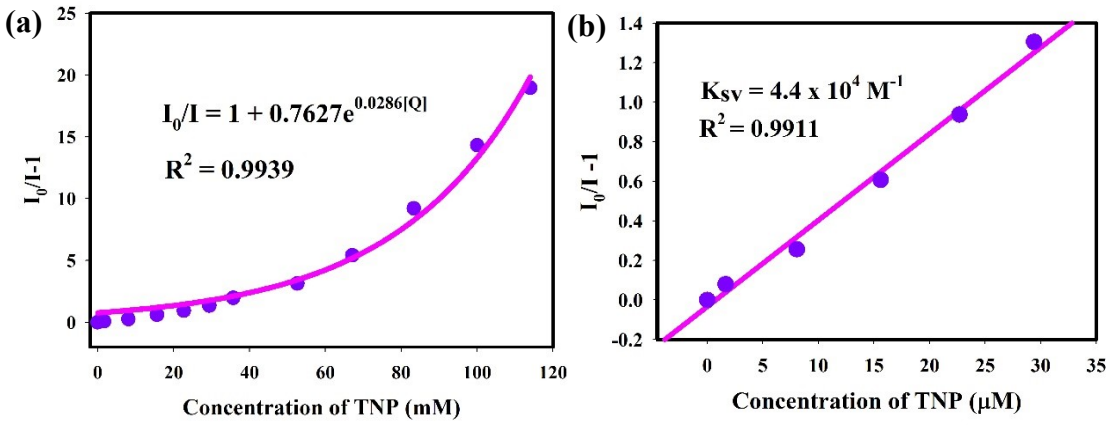

Fig. S20 (a) fitted curve of fluorescence intensity changes of CdPNMI emulsion upon the addition of TNP with different concentrations; (b) Stern−Volmer (SV) plot of fluorescence emissions for TNP.

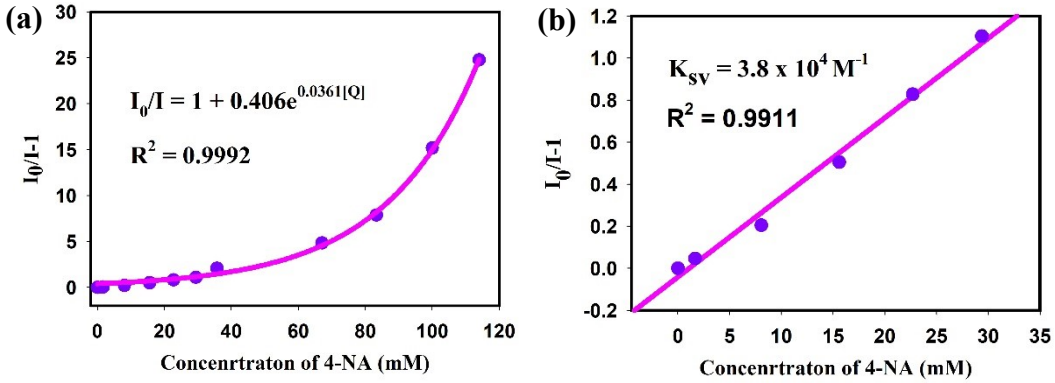

Fig. S21 (a) fitted curve of fluorescence intensity changes of CdPNMI emulsion upon the addition of 4-NA with different concentrations; (b) Stern−Volmer (SV) plot of fluorescence emissions for 4-NA.

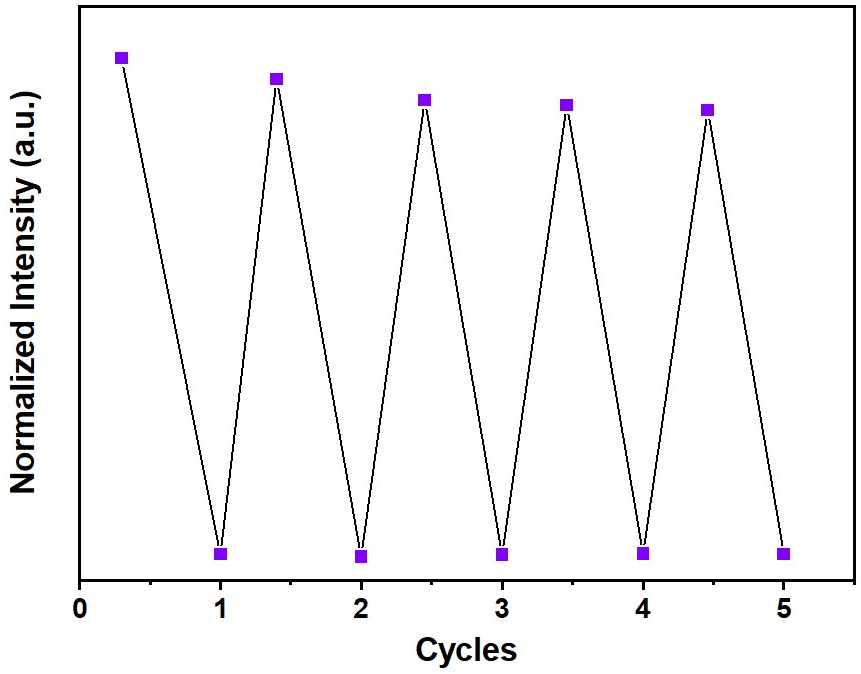

Fig. S22 The reversibility test of CdPNM for TNP.

(a)

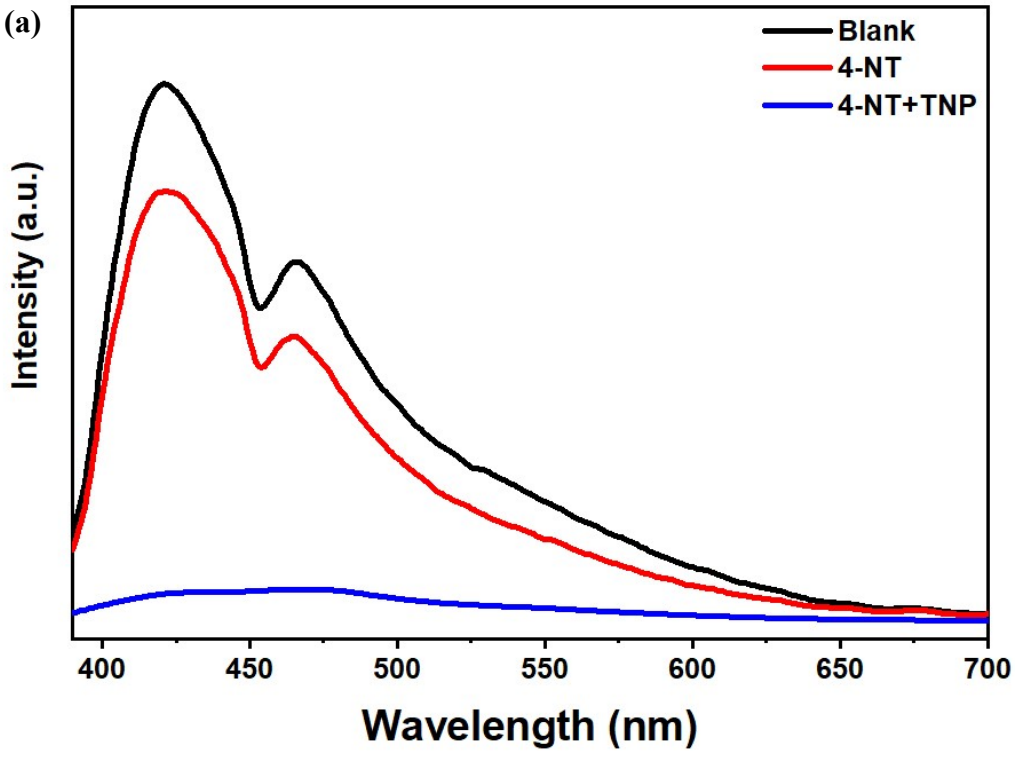

(b)

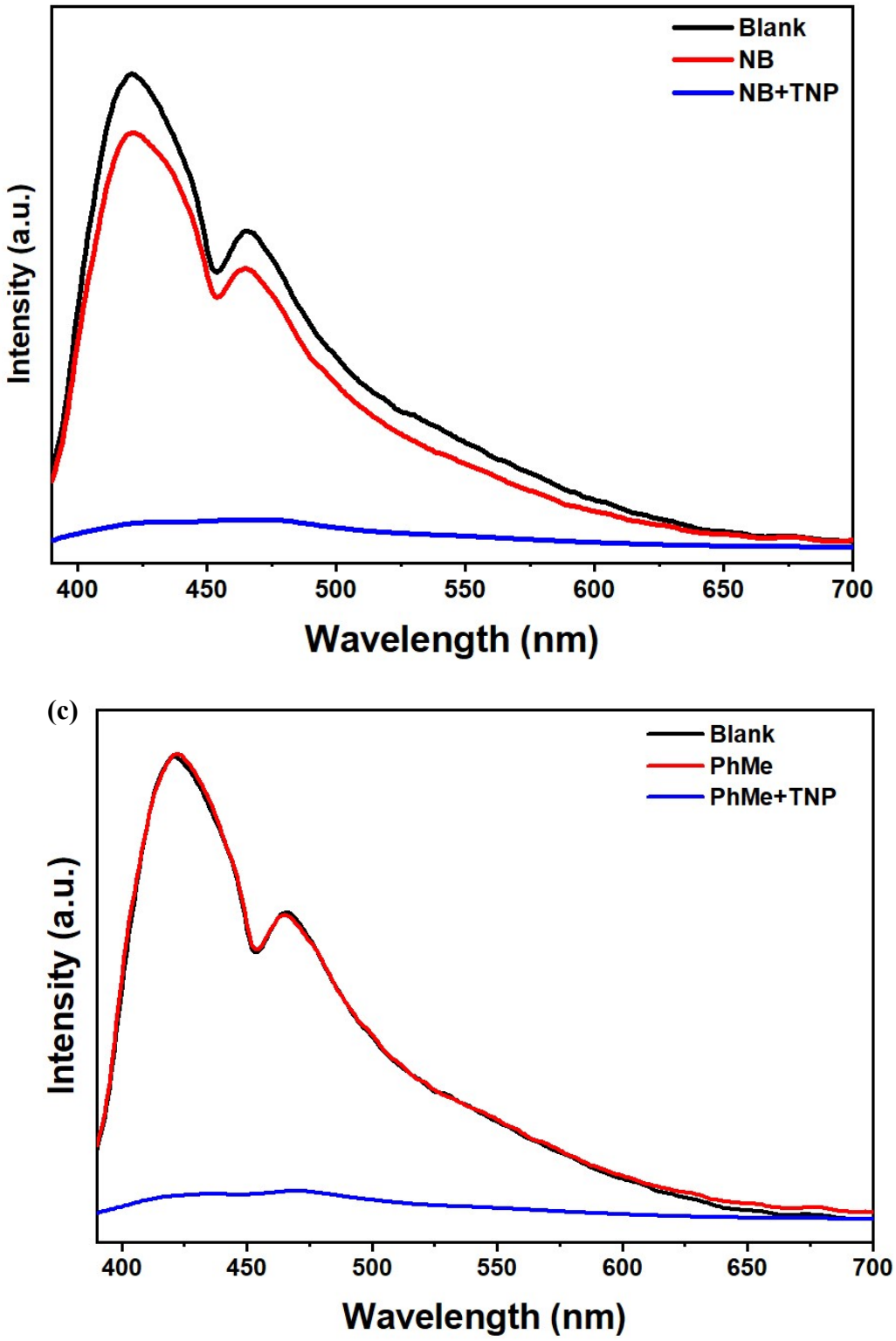

Fig. S23 The emission spectrum of CdPNMI emunlsion in DMA (black), the mixture incorporating organic compounds (red) and the mixture including organic compounds and TNP (blue).

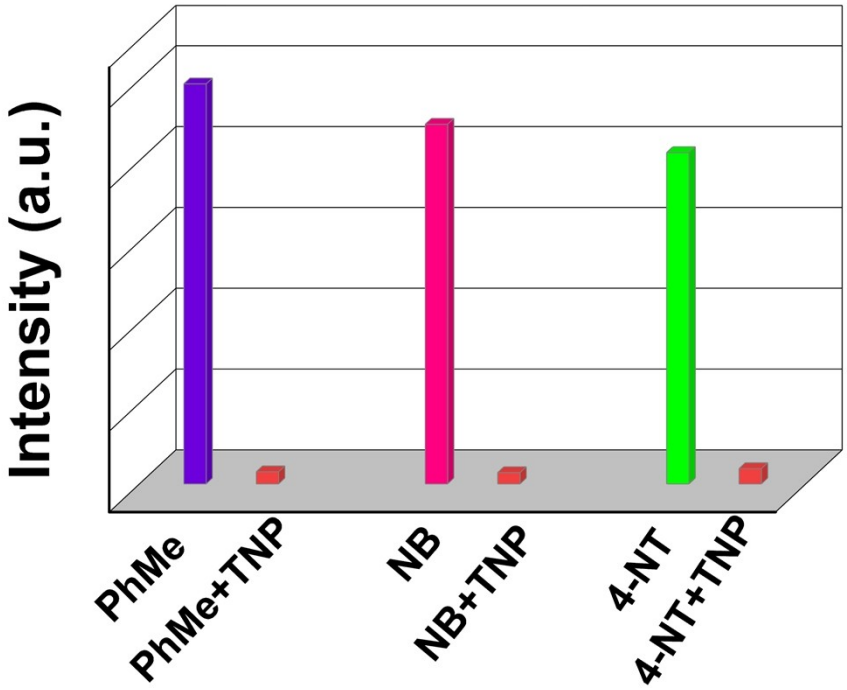

Fig. S24 The luminescence intensities change of CdPNMI in different quencher solution.

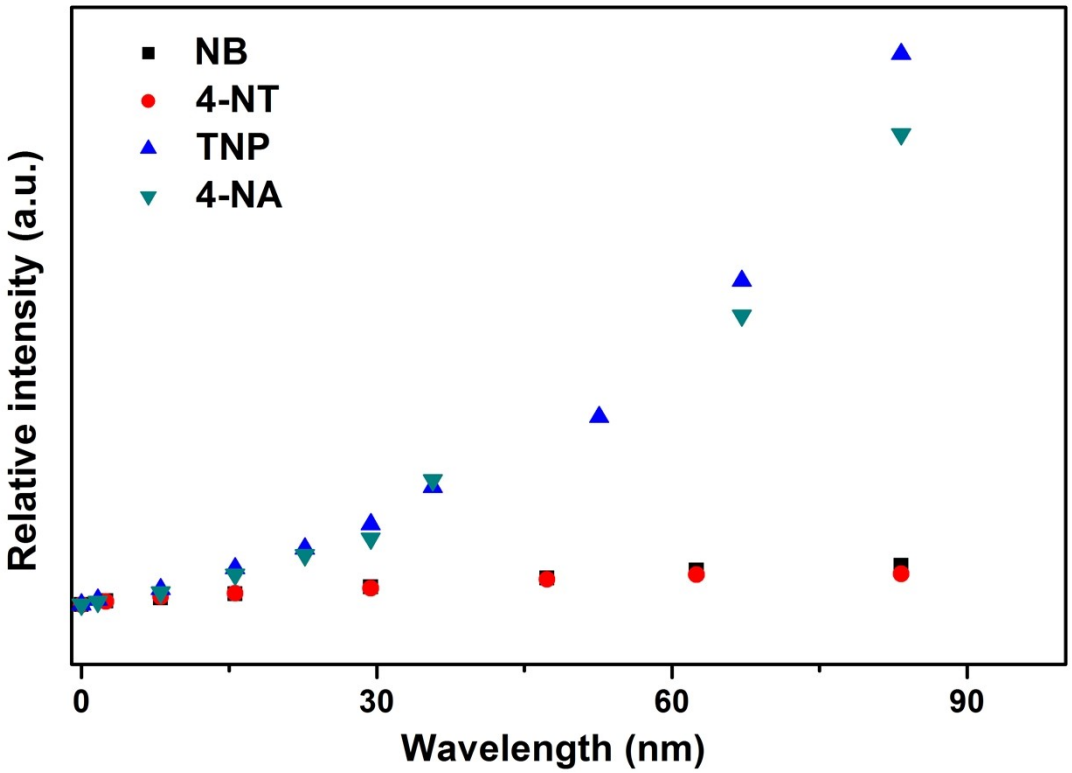

Fig. S25 Stern-Volmer plot of CdPNMI emulsion for nitro aromatic compounds

Computational Details

1. TDDFT calculation

To clarify the luminescent mechanism of CdPNMI, one fragment was extracted as model compound with one Cd_2O_2 ring and six complete organic ligands, which simulate the intact structure of CdPNMI (Fig. S26a).

All computations were conducted using the Gaussian16 software package [1]. The constructed structural model was calculated by performing time-dependent density functional theory (TDDFT) calculation with B3LYP hybrid function and 3-21g basis set. The optimized structure was used for calculating excited-state properties including excitation energies, oscillator strength, HOMO and LUMO.

(a)

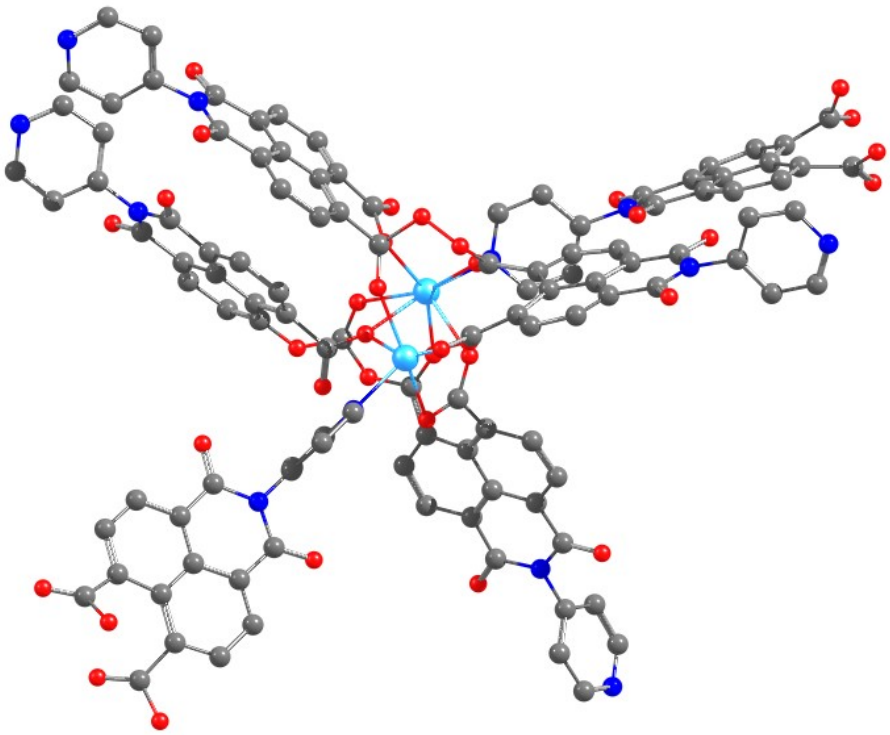

(b)

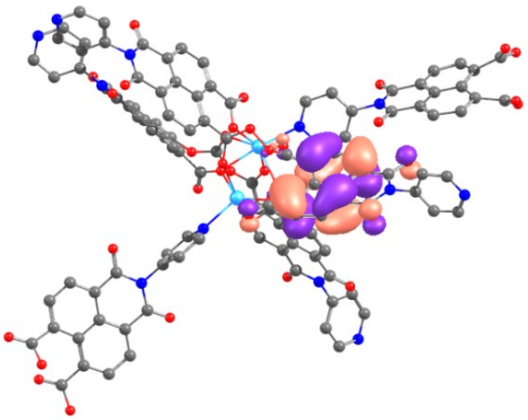

HOMO (π_1)

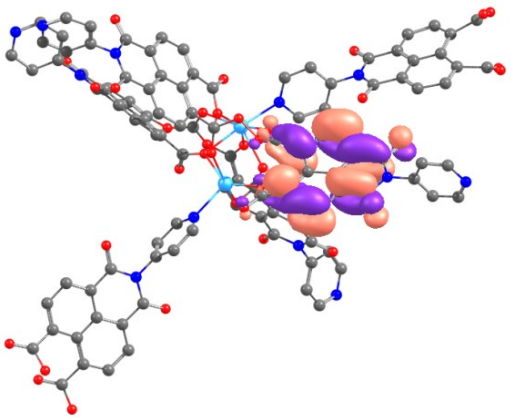

LUMO+5 (π_1*)

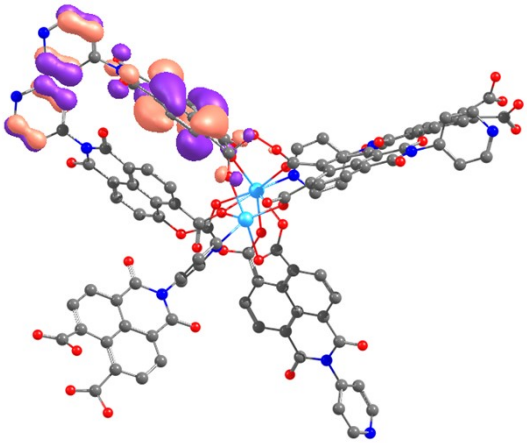

HOMO-4 (π_2)

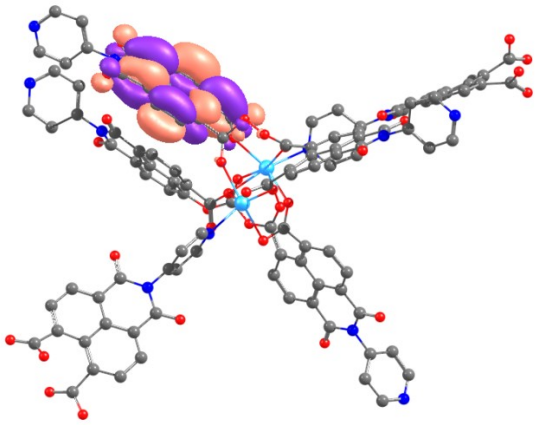

LUMO+2 (π_2*)

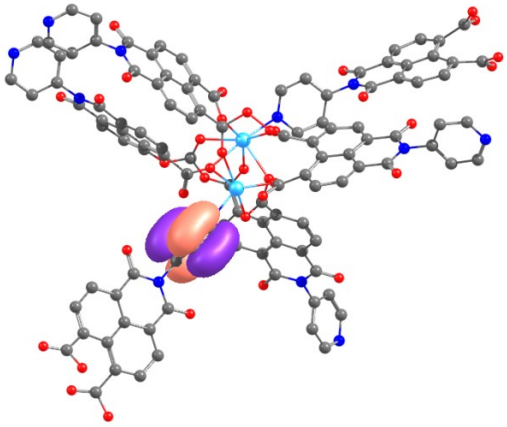

HOMO-13 (π_3)

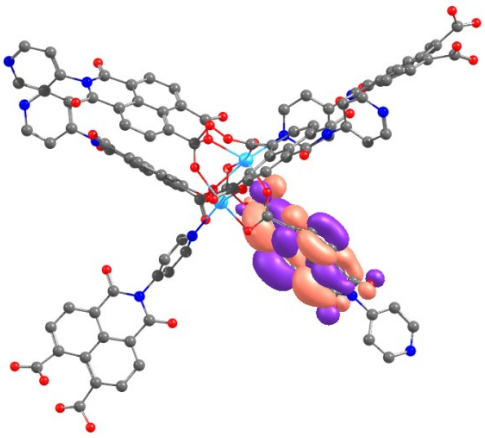

LUMO (π_3*)

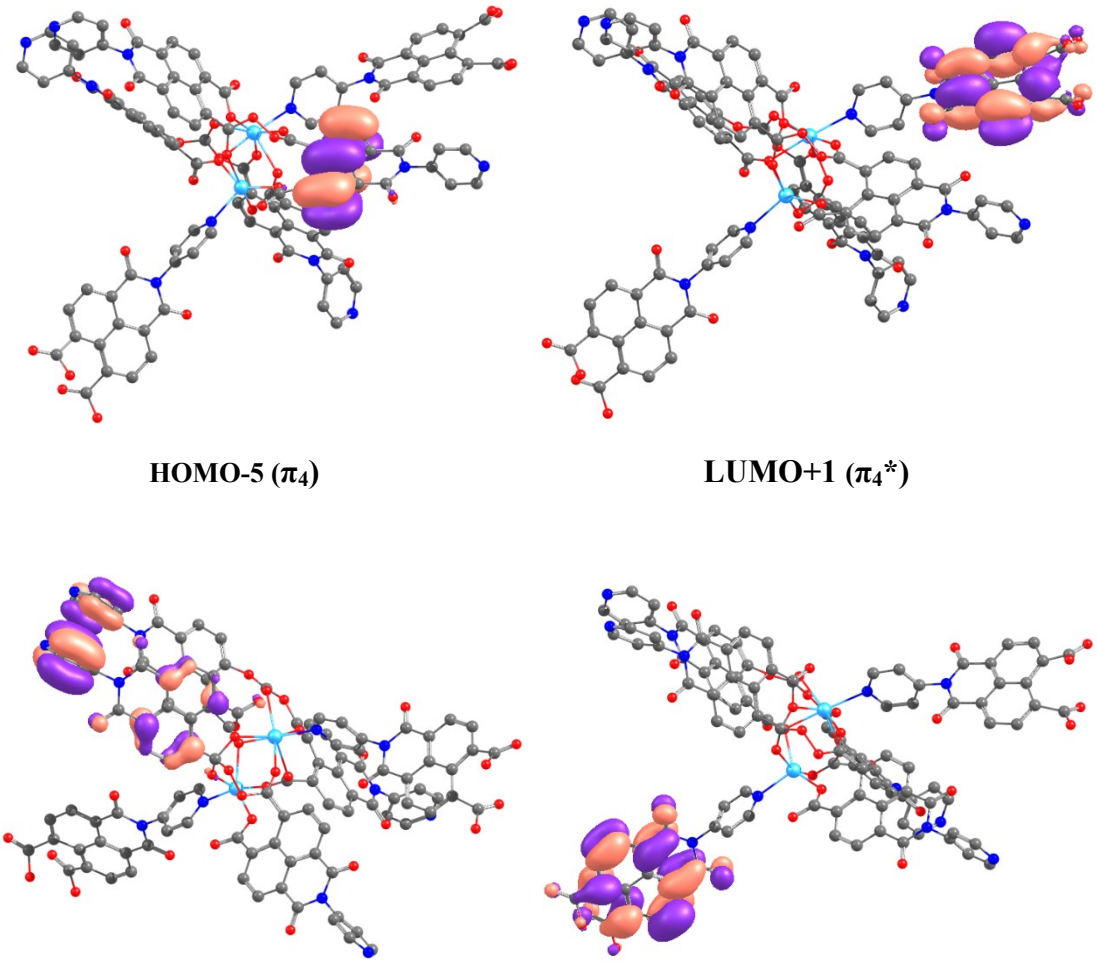

Fig. S26 (a) the calculated model of CdPNMI; (b) Contour plots of the frontier orbitals of CdPNMI model (color code: Cd, cyan; C, gray; O, red; N, blue; H atom is ignored for clarity)

Table S3 Excitation Energies (E, eV), Oscillator Strengths (f), Characteristics of Singly Occupied Molecular Orbitals (SOMOs) Summarized for Various Electron Transitions of CdPNMI.

Transitions	*E* (eV)	*f*	SOMO

$S_0 \rightarrow S_{CT1}(\pi\pi^*)$	4.5295	0.7007	$\pi_4 \rightarrow \pi_4^*$
$S_0 \rightarrow S_{CT2}(\pi\pi^*)$	4.5956	0.5198	$\pi_5 \rightarrow \pi_5^*$
$S_0 \rightarrow S_{LE1}(\pi\pi^*)$	4.6387	0.4036	$\pi_1 \rightarrow \pi_1^*$
$S_0 \rightarrow S_{LE2}(\pi\pi^*)$	4.6335	0.4046	$\pi_2 \rightarrow \pi_2^*$
$S_0 \rightarrow S_{CT3}(\pi\pi^*)$	4.6801	0.9280	$\pi_3 \rightarrow \pi_3^*$
$S_0 \rightarrow S_{CT4}(\pi\pi^*)$	4.7250	0.1170	$\pi_3 \rightarrow \pi_3^*$

Note: π_1-π_5 and π_1^*-π_5^* in the table S3 refer to the corresponding HOMO and LUMO in Fig. S26

2. DFT calculation

We conducted the calculation at the density functional theory (DFT) level. The B3LYP functional was used to carry out geometrical optimizations of the organic ligand PNMI, and the probed molecules including TNP, 4-NA, 4-NT, and NB. All-electron 6−31G* basis set was employed for all atoms. All calculations were implemented using the Gaussian 09 program package [2].

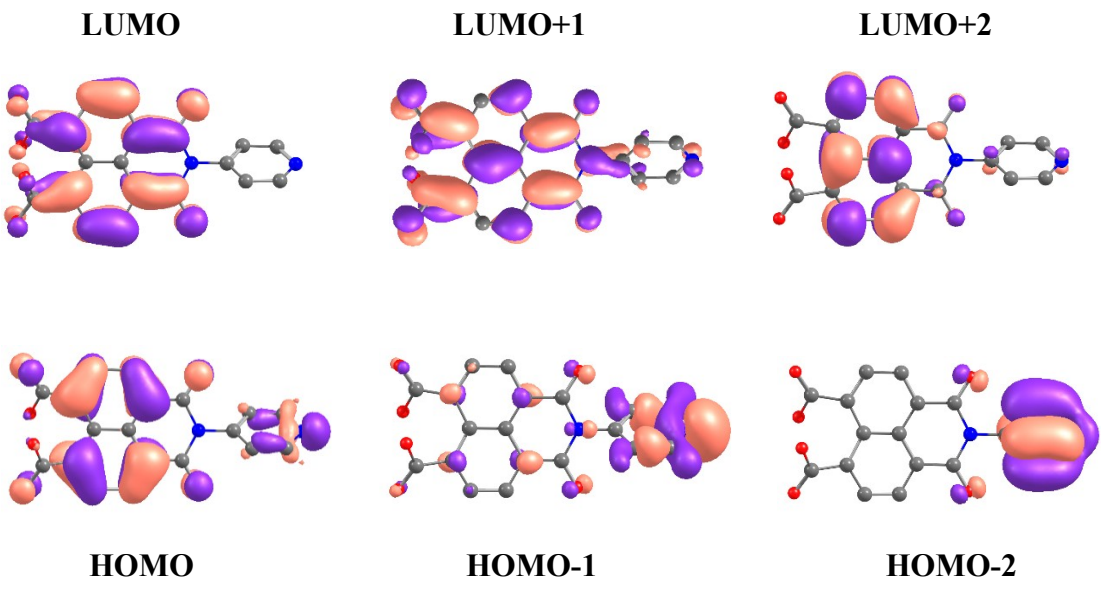

Fig. S27 Contour plots of the frontier orbitals of organic ligand (**PNMI**) model

Dyes absorption

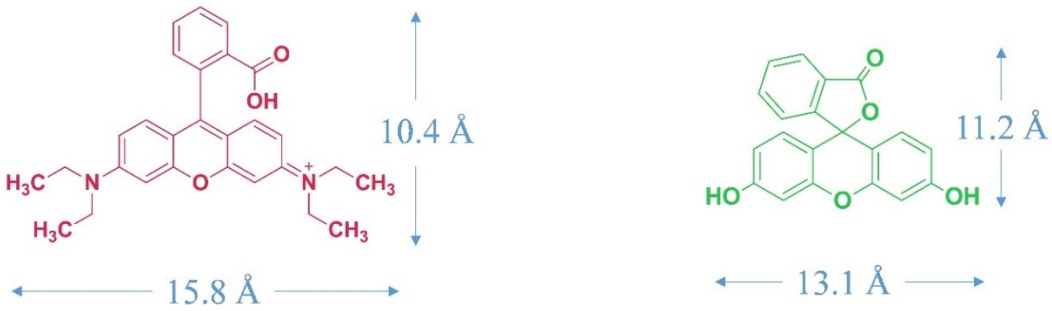

Fig. S28 the structure and size of Rhodamine B (red) and fluorescein (green) molecules.

The quantity of dyes absorption

calculate the quantity (q_e) of dyes (mg/g) adsorbed at equilibrium using the formula:

$$q_e = \frac{(C_0 - C_e)v}{m}$$

where C_0 and C_e (mg/L) are the initial and final concentrations of the adsorbates respectively, v is the volume of the solution used (mL) and m is the mass (g) of the adsorbents.

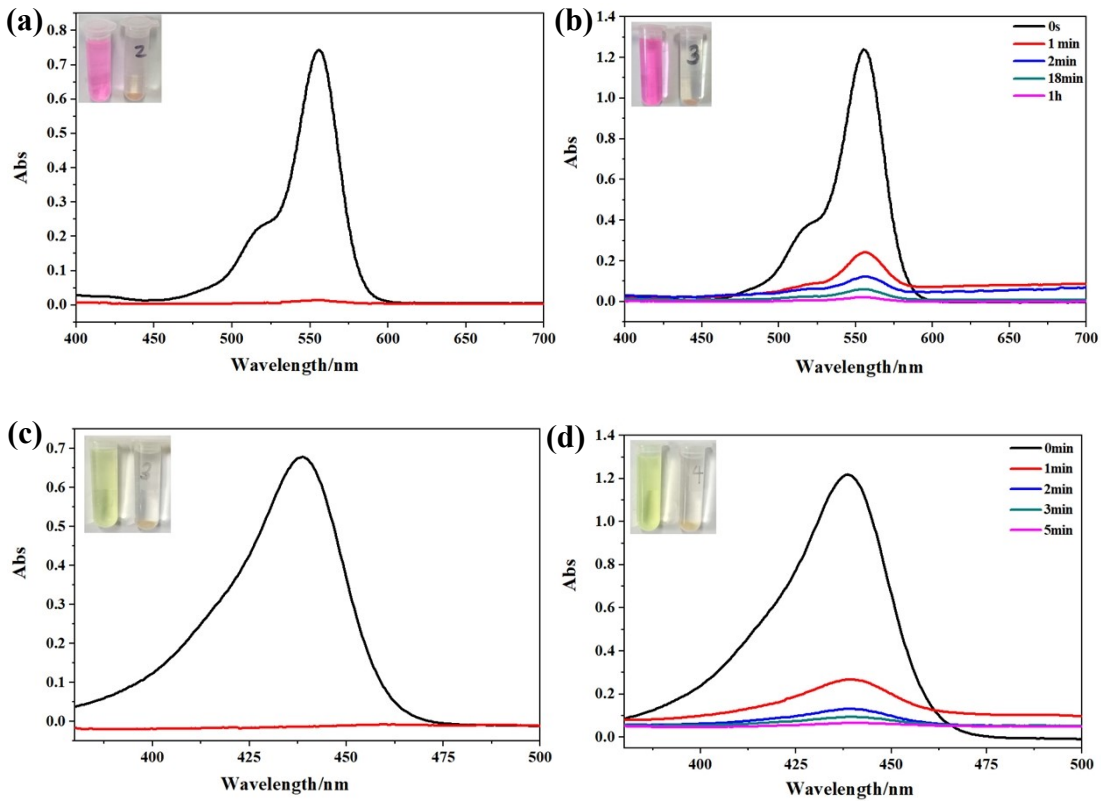

(e) (f)

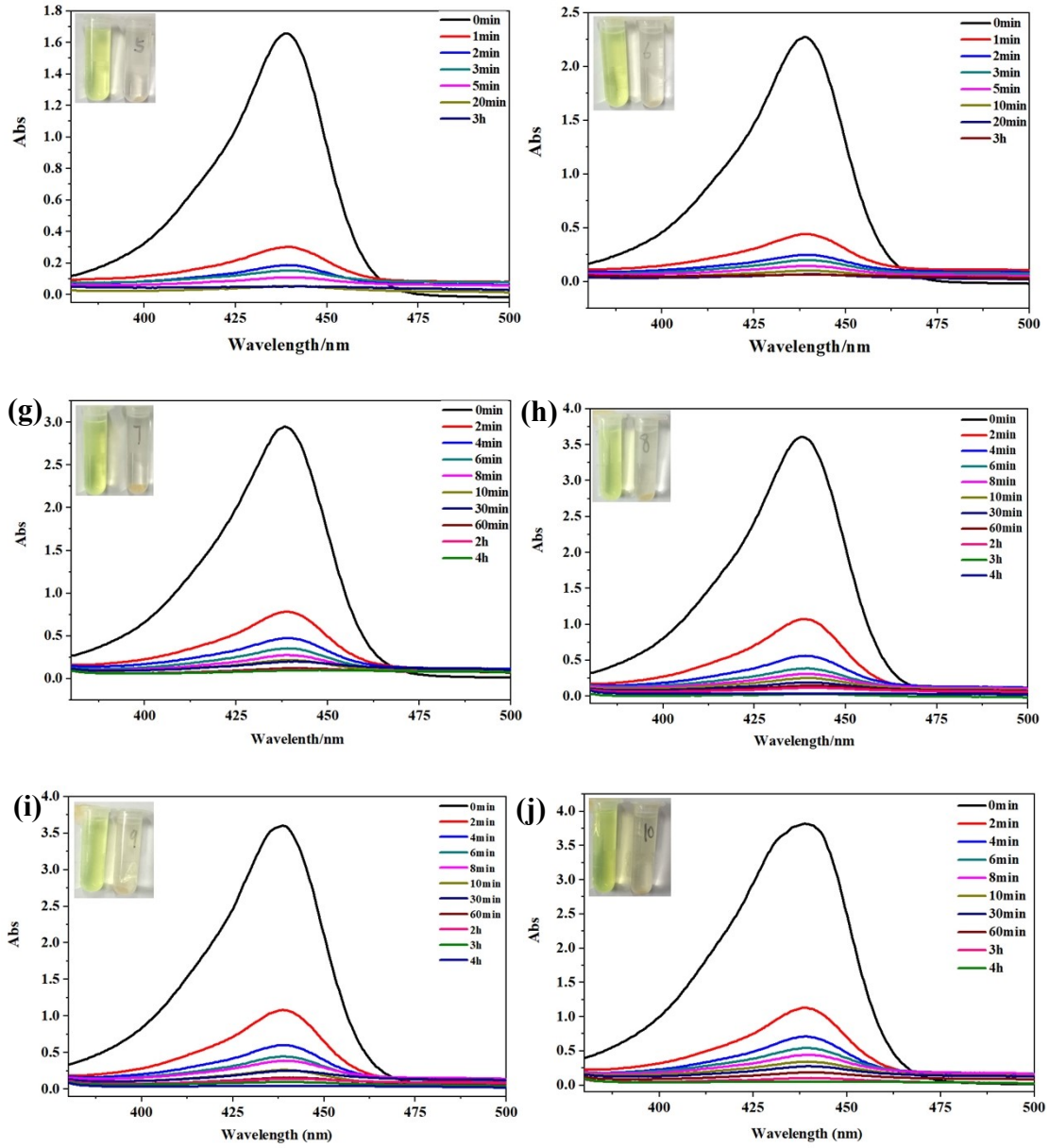

Fig. S29 Temporal evolution of UV/Vis absorption spectra of 20 mL acetone solution containing a) RhB (10 mg L^{-1}), b) RhB (15 mg L^{-1}), c) FITC (150 mg L^{-1}), d) FITC (200 mg L^{-1}), e) FITC (250 mg L^{-1}), f) FITC (300 mg L^{-1}), g) FITC (350 mg L^{-1}), h) FITC (400 mg L^{-1}), i) FITC (450 mg L^{-1}), j) FITC (500 mg L^{-1}) for CdPNMI adsorption. The photographs show the colours of the solution and crystal before and after organic dye adsorption.

Table S4 Absorption capacity of the reported adsorbents for FITC

NO.	Material	Absorbent	Adsorption capacity (mg g^{-1})	Ref.

1	herb	wild herb microparticles	2.91	3
2	Inorganic compound	goethite	66.46	4
3	Inorganic-ionic liquid complex	Montmorilloni-BMIM	1.918	5
4	hybrid	$(MV)[BiI_3Cl_2]$	793	6
5	complex	Co@MIL-125Ti@DE	622.84	7
6	MOF	MOF-808	480	8
7	MOF	NH_2-MIL-125	138	9
8	MOF	CdPNMI	1000	This work

Reference

1. GaussView, Version 6.1, Roy Dennington, Todd A. Keith, and John M. Millam, Semichem Inc., Shawnee Mission, KS, 2016.
2. Frisch, M. J.; Trucks, G. W.; Schlegel, H. B.; Scuseria, G. E.; Robb, M. A.; Cheeseman, J. R.; Scalmani, G.; Barone, V.; Mennucci, B.; Petersson, G. A. Gaussian 09, revision B.01; Gaussian, Inc.: Wallingford, CT, 2009.
3. G. M. Al-Senani and N. S. Al-Kadhi, *Int. J. Anal. Chem.*, 2020, **2020**, 8019274.
4. S. Pirillo, L. Cornaglia, M. L. Ferreira and E. H. Rueda, *Spectrochim. Acta A Mol. Biomol. Spectrosc*, 2008, **71**, 636-643.
5. A. Belbel, M. Kharroubi, J.-M. Janot, M. Abdessamad, A. Haouzi, I. K. Lefkaier and S. Balme, *Colloids Surf A Physicochem Eng Asp*, 2018, **558**, 219-227.
6. J. Wang, J. Zheng, S. T. Wang, J. Sun, Y. M. Guo, H. Wang, S. G. Huang, Y. D. Li and C. C. Wang, *Mater. Lett.*, 2019, **254**, 419-422.
7. A. Sheng, J. Li, H. Li, Q. Wang, C. Zhao and Z. Cheng, *Mater. Lett.*, 2024, **365**, 136463.
8. S. Jia, S. Song and X. Zhao, *Appl Organomet Chem.* , 2021, **35**, e6314.
9. J. Huang, D. Huang, F. Zeng, L. Ma and Z. Wang, *J. Mater. Sci.*, 2021, **56**, 3127-3139.